Quantum state engineering using weak measurements

Qiang Hu, Taximaiti Yusufu,* and Yusuf Turek†
School of Physics and Electronic Engineering, Xinjiang Normal University, Urumqi, Xinjiang 830054, China

(Received 1 November 2021; accepted 25 January 2022; published 11 February 2022)

State preparation via postselected weak measurements in a three-wave mixing process is studied. We assume the signal input mode is prepared in a vacuum state, coherent state, or squeezed vacuum state, while the idler input is prepared in a weak coherent state and passes the medium characterized by the second-order nonlinear susceptibility. It is shown that when the single photon is detected at one of the output channels of the idler beam's path, the signal output channel is prepared in a single-photon Fock state, single-photon-added coherent state, or single-photon-added squeezed vacuum state with very high fidelity, depending upon the input signal states and related controllable parameters. The properties of squeezing, signal amplification, second-order correlation, and the Wigner functions of the weak-measurement-based output states are also investigated. Our scheme promises to provide an alternate effective method for producing useful nonclassical states in quantum information processing.

DOI: 10.1103/PhysRevA.105.022608

I. INTRODUCTION

New state generation and its optimization have significant importance in quantum information processing [1–6]. Plenty of research works have studied various quantum states and have proposed schemes for generating them. Particular interest has been devoted to Fock states [7–9], Schrödinger's cat states [10–18], squeezed states [19], photon-number states [20–26], binomial states [27–29], and squeezed-state excitations [30–33]. Another interesting class of nonclassical states that includes photon-added coherent states [34] and photon-subtracted or -added squeezed states [35] has been a subject of interest since these states also have potential for many related quantum information processing applications [36–39]. Those states can be produced by repeated applications of photon creation or annihilation operators [40] on a given state [41–45].

We know that proposing feasible schemes to generate specific quantum states and their implementations in the laboratory is an exciting and challenging task for researchers. In specific quantum state generation processes we usually use the conditional measurement since it useful to control the desired parameters to produce the desired quantum states [46–53]. The weak measurement proposed in 1988 [54] by Aharonov *et al.* is a typical conditional measurement characterized by postselection and a weak value. The weak-measurement theory has various applications (see [55] and references therein), and it was recently widely used for state-optimization problems [56–58]. One of the authors of this work studied state optimization by using weak measurements [59–61] and showed that the postselected weak measurements really can change the inherent properties of the given states. Furthermore, in a recent work [62], the authors proposed a theoretical scheme to amplify the single-photon nonlinearity using weak measurements implemented in a cross-Kerr-interaction medium characterized by third-order nonlinear susceptibility $\chi^{(3)}$, and its experimental realization was given in [63]. On the other hand, Shikano and his collaborators [64] studied the generation of phase-squeezed optical pulses with large coherent amplitudes by postselection of a single photon based on the same setup as in Ref. [62]. Most recently, the protocols for steering the state of the quantum system from an arbitrary initial state toward any chosen state was proposed using weak measurements [65,66]. The above-mentioned results also indicated the potential usefulness of postselected weak measurements in quantum state engineering processes. Thus, in order to provide alternate methods for the implementation of the related quantum information processes, specific quantum state generation via weak measurements is worth studying.

In this paper, we introduce a scheme to generate some nonclassical states such as a single-photon Fock state, a single-photon-added coherent (SPAC) state, and a single-photon-added squeezed vacuum (SPASV) state in a three-optical-wave mixing process via postselected weak measurements [54]. In order to achieve our goal, we consider the signal and idler beams as the pointer (measuring system) and measured system, respectively. We assume that initially, the measured system is prepared in a very weak coherent state, while the pointer (signal) state is prepared in a coherent or squeezed vacuum state. The moderate-intensity pump field is treated as classical and the weak coupling between the pointer and measured system is realized by a beta barium borate (BBO) nonlinear crystal which can generate entanglement between them. By properly choosing the pre- and postselection states of the measured system and detecting one photon in one of the outputs of the idler mode, the output channel of the pointer is prepared in the desired state with high purity for controllable parameters. We found that if our input pointer state is prepared in a coherent (squeezed vacuum) state, then we can generate a SPAC (SPASV) state with very high fidelity

*taxmamat_84@sina.com
†Corresponding author: yusufu1984@hotmail.com

accompanied by a small successful postselection rate. Our results indicated that in our scheme we also can generate a single-photon Fock state if the initial pointer state is prepared in the vacuum state. To further confirm the identities of those generated states we also investigate their related properties such as squeezing, second-order correlations, and Wigner functions. Interestingly, we found that the generated SPAC state in our scheme has advantages to increase the signal-to-noise ratio (SNR) in postselected weak measurements over the nonpostselected case.

This paper is organized as follows. Section II presents the basic scheme for generating nonclassical states in a three-wave mixing process via the postselected weak-measurement technique. The generation of SPAC and SPASV states and their verification are discussed in Secs. III and IV, respectively. In Sec. III, we also investigate the advantages of postselected weak measurements in the signal-amplification process over the nonpostselected case for the SPAC state by adjusting the low value of the measured system observables. Finally, a summary and concluding remarks are given in Sec. V.

II. MODEL SETUP FOR STATE GENERATION VIA POSTSELECTED WEAK MEASUREMENTS

The Hamiltonian of a three-wave mixing device [67], under the rotating-wave approximation, neglecting external drive and signal fields, is

$$H = \hbar\omega_s a^\dagger a + \hbar\omega_i b^\dagger b + \hbar\omega_p c^\dagger c + i\hbar\chi^{(2)}(a^\dagger b^\dagger c - abc^\dagger), \tag{1}$$

where a, b, and c are the annihilation operators of the signal, idler, and pump with frequencies ω_s, ω_i, and ω_p, respectively, and $\chi^{(2)}$ is the coupling strength characterized by a second-order nonlinear susceptibility of the BBO crystal. This Hamiltonian can describe the process of nondegenerate parametric down-conversion whereby a photon of the pump field is converted into two photons, one for each of modes a and b [67]. Using the parametric approximation, assuming that the pump field is a strong coherent state of the form $|\gamma e^{-i\omega_p t}\rangle$ [67], we can rewrite the above Hamiltonian in the interaction picture with $\omega_p = \omega_i + \omega_s$ as

$$H_I = i\hbar\xi(a^\dagger b^\dagger - ab), \tag{2}$$

where $\xi = \gamma\chi^{(2)}$. Further, the above Hamiltonian is equivalent to

$$H_I = \hbar\xi(A \otimes p - B \otimes q) \tag{3}$$

if we introduce

$$B = \frac{i}{\sqrt{2}}(b - b^\dagger), \quad A = \frac{1}{\sqrt{2}}(b^\dagger + b), \tag{4}$$

$$q = \frac{1}{\sqrt{2}}(a^\dagger + a), \quad p = \frac{i}{\sqrt{2}}(a^\dagger - a), \tag{5}$$

with $[A, B] = i$ and $[q, p] = i$, respectively. The two terms in the Hamiltonian, Eq. (3), are in the form we usually use in weak-measurement problems [54]. In this work the signal beam with variables q and p is the pointer, and the idler beam with variables A and B is the measured system.

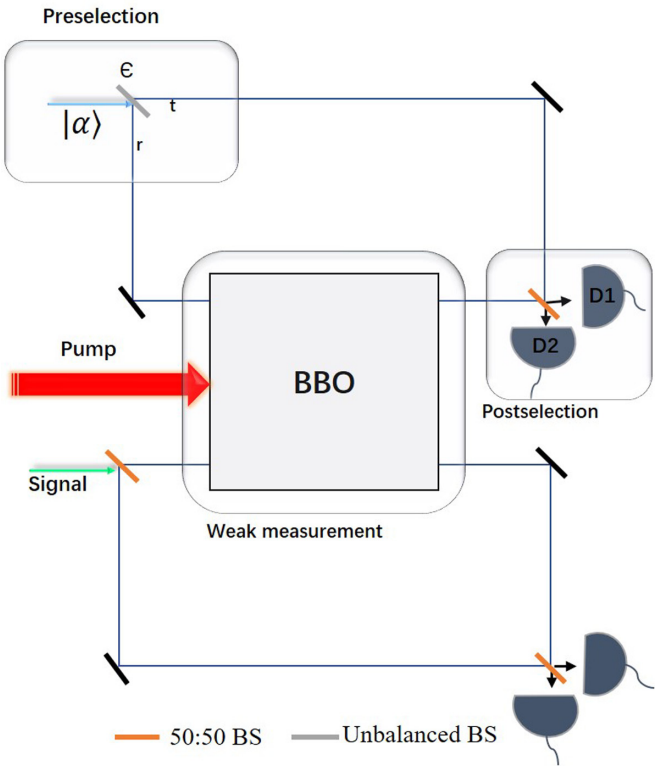

FIG. 1. Schematics of non-Gaussian state generation in a three-wave mixing process using postselected weak measurements. This model consists of two Mach-Zehnder interferometers. The signal and idler beams act as the pointer and measured system, respectively. The preselection state is prepared by the weak coherent state $|\alpha\rangle$ passing through the unbalanced beam splitter (BS) with deviation ϵ, and the signal beam is initially prepared in some specific states. The BBO crystal plays the role of realizing the weak interaction between the pointer and measured system. The 50:50 BS in the upper Mach-Zehnder interferometer plays the role of postselection, and the desired conditional quantum state is generated in the output mode of the signal beam after we detect one photon by the second photon detector (D2) in the idler beam's path.

The schematic setup of our state-generation model is shown in Fig. 1. As we can see from Fig. 1, there are two Mach-Zehnder interferometers in our setup, and the beam splitters have very important roles in the implementation of our scheme. Beam splitters are basic manipulations in classical and quantum optics to split and mix the optical beams. The input and output relations of beam splitters can be described by Lie algebra [68]. In the Heisenberg picture, the photon annihilation operators of the output beam b_k $(k = 1, 2)$ can be connected to input beam's annihilation operators a_k as

$$b_k = \sum_{j=1}^{2} V_{kj} a_j, \tag{6}$$

where V_{kj} is an element of the scattering matrix

$$V = \begin{pmatrix} \cos\vartheta\, e^{i\varphi_t} & \sin\vartheta\, e^{i\varphi_r} \\ -\sin\vartheta\, e^{-i\varphi_r} & \cos\vartheta\, e^{-i\varphi_t} \end{pmatrix}. \tag{7}$$

Here $T = \cos\vartheta\, e^{i\varphi_t}$ and $R = \sin\vartheta\, e^{i\varphi_r}$ are the transmittance and reflectance of the beam splitter, respectively. If $\varphi_r = \frac{\pi}{2}$, $\varphi_t = 0$ and $\vartheta = \frac{\pi}{4}$, then it becomes a 50:50 beam splitter.

We assume that initially, the measured system (idler beam) is prepared in a weak coherent state with a low amplitude ($\alpha \ll 1$) and the signal beam is separately prepared in some specific states such as the squeezed vacuum state or coherent state. In the upper optical path of our scheme, we assume that the first beam splitter is slightly imbalanced with a small deviation ϵ from 50:50 so that the preselection state of the measured system can be written as [69]

$$|\psi_i\rangle = \left|\frac{\alpha}{\sqrt{2}}(1-\epsilon)\right\rangle_t \left|\frac{i\alpha}{\sqrt{2}}(1+\epsilon)\right\rangle_r. \tag{8}$$

Here the subscripts t and r indicate the transmitted and reflected beams from the beam splitter. Then, the three-wave mixing is realized by the nonlinear BBO crystal, which plays a role in implementing the weak-measurement process. In this process, the input photon annihilates and produces two new mutually entangled photons. The unitary evolution operator corresponding to the interaction Hamiltonian $H_I = \hbar g(A \otimes p - B \otimes q)$ which can be implemented by the BBO crystal is

$$U = \exp\left(-\frac{i}{\hbar}\int_0^t H_I d\tau\right) = \exp\left(-ig[A \otimes p - B \otimes q]\right), \tag{9}$$

where $g = \xi t$. Actually, the squeezing operator can generate the two-mode vacuum squeezed state [67]. Here g can be considered a squeezing parameter which depends on pump intensity, the crystal length, and its nonlinear coefficients. In our scheme, the coupling between the idler and signal beams is weak, and it can be characterized by g. As mentioned above, when the pump is an intense beam, we can treat it as a classical field, and an interaction between the signal and idler such as $e^{g(a^\dagger b^\dagger - ab)}$ can be realized [44]. Thus, the pump can be moderate intensity for a not narrow crystal so that $g < 1$; then we can take the limit of weak nonlinearity. Following the experimental work [44], we set $g = 0.105$ throughout this work. We can thus rewrite the above unitary evolution operator U as

$$U \simeq I - ig(A \otimes p - B \otimes q). \tag{10}$$

If we assume that the initial states of the system and pointer are $|\psi_i\rangle$ and $|\phi\rangle$, after the unitary evolution the total system state becomes

$$|\Psi\rangle = U|\psi_i\rangle \otimes |\phi\rangle \approx [I - ig(A \otimes p - B \otimes q)]|\psi_i\rangle \otimes |\phi\rangle. \tag{11}$$

This is the total system state before it arrives at the second beam splitter in our model (see Fig. 1). In our scheme the second beam splitter is 50:50 with 50% transmission and 50% reflection. We undertake a postselection of the idler beam that is accomplished by detectors in the upper optical paths. Assume that the second photon detector (D2) detects one photon and the first photon detector (D1) does not detect a click, i.e., $|1\rangle_{2d}|0\rangle_{1d}$. This postselection process can be described by

$$\begin{aligned}|\psi_f\rangle_{2d} &= a_{2d}^\dagger|0\rangle_r|0\rangle_t \\ &= \frac{1}{\sqrt{2}}(|0\rangle_r|1\rangle_t - i|1\rangle_r|0\rangle_t),\end{aligned} \tag{12}$$

where

$$a_{2d} = \frac{1}{\sqrt{2}}(a_t + ia_r), \tag{13a}$$

$$a_{1d} = \frac{1}{\sqrt{2}}(ia_t + a_r) \tag{13b}$$

are the field-operator relations between the input and output modes of the beam-splitter transformation. After making the postselection with the postselected state $|\psi_f\rangle$ in Eq. (11), we can obtain the non-normalized form of the final state of the pointer (signal beam), which reads

$$\begin{aligned}|\Phi\rangle &= \langle\psi_f|\psi_i\rangle[1 - ig(\langle A\rangle_w p - \langle B\rangle_w q)]|\phi\rangle \\ &= \langle\psi_f|\psi_i\rangle\left[1 - \frac{g\alpha}{\sqrt{2}}a - \frac{g}{\sqrt{2}\alpha\epsilon}a^\dagger\right]|\phi\rangle,\end{aligned} \tag{14}$$

where

$$\langle A\rangle_w = \frac{\langle\psi_f|\hat{A}|\psi_i\rangle}{\langle\psi_f|\psi_i\rangle} = \frac{\alpha}{2} - \frac{1}{2\alpha\epsilon}, \tag{15}$$

$$\langle B\rangle_w = \frac{\langle\psi_f|\hat{B}|\psi_i\rangle}{\langle\psi_f|\psi_i\rangle} = \frac{i}{2\alpha\epsilon} + i\frac{\alpha}{2} \tag{16}$$

are the weak values of A and B, respectively. The probability of finding one photon at D2 and no photon at D1 is

$$P_s = |\langle\psi_f|\psi_i\rangle|^2 = |\alpha\epsilon|^2. \tag{17}$$

As we can see, the success probability of the postselection P_s depends on the imbalance ϵ caused by the small difference between the reflection and transmission coefficients of the beam splitter in the upper interferometer and weak coherent-state amplitude α of the idler input state. From Eqs. (15) and (16), it can be seen that the weak values are generally complex and can take large values when the preselected state $|\psi_i\rangle$ and postselected states $|\psi_f\rangle$ are almost orthogonal. The magnitudes of the weak idler-input-state amplitude α, beam-splitter deviation ϵ, and coupling coefficient g are all controllable in optical experiments. Thus, we can manipulate and change the inherent properties of the output signal state $|\Phi\rangle$ by adjusting these parameters. In the remaining parts of this paper, we study the state generation and its verification processes by taking the initial signal input sate $|\phi\rangle$ as the coherent state and vacuum squeezed state, respectively.

III. GENERATION OF THE SPAC STATE

In this section, we assume that the initial signal input state is prepared in a coherent state, which is defined as

$$|\phi\rangle = |\beta\rangle = D(\beta)|0\rangle, \tag{18}$$

where $\beta = |\beta|e^{i\theta}$ is a complex number. For this case, the output state of the signal, i.e., Eq. (14), reads

$$|\Theta\rangle = \mathcal{N}[\kappa_1|\beta\rangle - \kappa_2 a^\dagger|\beta\rangle]. \tag{19}$$

Here

$$\mathcal{N} = \{|\kappa_1|^2 + |\kappa_2|^2(1 + |\beta|^2) - 2\mathrm{Re}[\kappa_1\kappa_2^*\beta]\}^{-\frac{1}{2}} \tag{20}$$

is the normalization constant, $\kappa_1 = 1 - \frac{g\beta\alpha}{\sqrt{2}}$, and $\kappa_2 = \frac{g}{\sqrt{2}\alpha\epsilon}$. It is very clear from Eq. (19) that the output signal state is a superposition of the coherent state $|\beta\rangle$ and SPAC state $a^\dagger|\beta\rangle$.

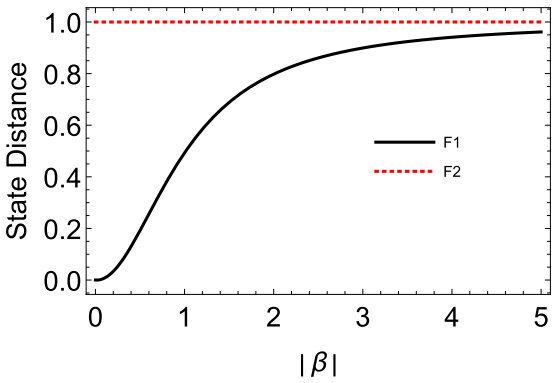

FIG. 2. State distance between the coherent state $|\beta\rangle$, SPAC state $\frac{a^\dagger|\beta\rangle}{\sqrt{1+|\beta|^2}}$, and $|\Phi\rangle$. Here we take $\theta = 0$, $g = 0.105$, $\alpha = 0.01$, and $\epsilon = 0.1$.

As mentioned, since the parameters g, α, ϵ, and β are adjustable, the dominance of the coherent state $|\beta\rangle$ and SPAC state $a^\dagger|\beta\rangle$ can be completely controlled by adjusting the related parameters. From Eq. (19), we can see that if $\kappa_2 \gg \kappa_1$, the state $|\Theta\rangle$ reduces to the SPAC state $|1,\beta\rangle = \frac{a^\dagger|\beta\rangle}{\sqrt{1+|\beta|^2}}$. The SPAC state was initially proposed by Agarwal and Tara in 1991 [34] and was first experimentally implemented in 2004 [41]. The SPAC state has many applications in quantum information processes, including quantum communication [70], quantum key distribution [37,38,71,72], and quantum digital signatures [39]. In the next sections we extend the discussions about the verification of the conditional output state $|\Theta\rangle$.

A. State distance

In quantum information theory, the quantification of the distance of two quantum states described by density operators ρ and σ can be characterized by the quantum fidelity (the so-called Uhlmann-Jozsa fidelity), which is defined as [73]

$$F = (Tr\sqrt{\sqrt{\rho}\sigma\sqrt{\rho}})^2. \tag{21}$$

If both states are pure, i.e., $\rho = |\psi\rangle\langle\psi|$ and $\sigma = |\phi\rangle\langle\phi|$, then

$$F = |\langle\psi|\phi\rangle|^2. \tag{22}$$

This quantity is, indeed, a natural candidate for the state distance since it corresponds to the closeness of states in the natural geometry of the Hilbert space. If $F = 0$, the states are orthogonal or called something totally different (i.e., perfectly distinguishable). If $F = 1$, then the two states are completely the same, $|\psi\rangle = |\phi\rangle$.

Here, in order to study the similarity of the output signal states $|\Theta\rangle$ between the coherent state $|\beta\rangle$ and the normalized SPAC state $|1,\alpha\rangle$, the fidelities between $|\beta\rangle$, $|1,\alpha\rangle$, and $|\Theta\rangle$ are calculated, and the results are given by

$$F_1 = |\langle\beta|\Theta\rangle|^2 = |\mathcal{N}(\kappa_1 - \kappa_2\beta^*)|^2, \tag{23}$$

$$F_2 = |\langle 1,\alpha|\Theta\rangle|^2 = \frac{|\mathcal{N}|^2|\kappa_1\beta - \kappa_2(1+|\beta|^2)|^2}{1+|\beta|^2}, \tag{24}$$

respectively. In Fig. 2, we plot fidelities F_1 and F_2 as a function of the coherent-state parameter $|\beta|$ for other fixed system parameters. In Fig. 2, the red dashed line shows the closeness between the output signal state and the SPAC state, and it can be seen that the fidelity of these two states always remains a constant value ($F = 1$) for all $|\beta|$. Figure 2 also indicates that F_1 increases from zero to unity as $|\beta|$ increases. It can be seen that when α and ϵ are much less than 1 and $|\beta|$ is smaller, we can deduce that $\kappa_2 \gg \kappa_1$. Under this condition our generated output signal state is exactly the SPAC state.

B. Second-order correlation and the Mandel factor

Here we study the second-order correlation function $g^{(2)}(0)$ and the Mandel factor Q_m of our generated signal state $|\Theta\rangle$. The second-order correlation function of a single-mode radiation field is defined as

$$g^{(2)}(0) = \frac{\langle a^{\dagger 2}a^2\rangle}{\langle a^\dagger a\rangle^2}. \tag{25}$$

Its relation to the Mandel factor Q_m is

$$Q_m = \langle a^\dagger a\rangle[g^{(2)}(0) - 1]. \tag{26}$$

If $0 \leqslant g^{(2)}(0) < 1$ and $-1 \leqslant Q_m < 0$ simultaneously, the corresponding radiation field has sub-Poissonian statistics and is more nonclassical. We have to remember that the Mandel factor Q_m can never be smaller than -1 for any radiation field, and negative Q_m values, which are equivalent to sub-Poissonian statistics, cannot be produced by any classical field.

The second-order correlation function $g^{(2)}(0)$ and the Mandel factor Q_m of our generated output signal state $|\Theta\rangle$ are given as [74]

$$g^{(2)}(0) = \frac{\langle\Theta|a^\dagger a^\dagger aa|\Theta\rangle}{\langle\Theta|a^\dagger a|\Theta\rangle^2}, \tag{27}$$

$$Q_m = \langle\Theta|a^\dagger a|\Theta\rangle[g^2(0) - 1], \tag{28}$$

respectively, with

$$\langle\Theta|a^{\dagger 2}a^2|\Theta\rangle = |\mathcal{N}|^2\{|\kappa_1|^2|\beta|^4 - 2\kappa_2^*\kappa_1\mathrm{Re}(2|\beta|^2\beta + |\beta|^4\beta) + |\kappa_2|^2(5|\beta|^4 + |\beta|^6 + 4|\beta|^2)\}, \tag{29}$$

and

$$\langle\Theta|a^\dagger a|\Theta\rangle = |\mathcal{N}|^2\{|\kappa_1|^2|\beta|^2 - 2\kappa_2^*\kappa_1\mathrm{Re}(\beta + |\beta|^2\beta) + |\kappa_2|^2(3|\beta|^2 + |\beta|^4 + 1)\}. \tag{30}$$

In Fig. 3, we plot $g^{(2)}(0)$ and Q_m as functions of the coherent-state parameter β by fixing the other parameters to $\theta = 0$, $g = 0.105$, $\alpha = 0.01$, and $\epsilon = 0.1$. As observed in Fig. 3, $0 \leqslant g^{(2)}(0) < 1$, and $-1 \leqslant Q_m < 0$ for all plotted regions. This means that our generated signal output field has sub-Poisson statistics which is possessed by only nonclassical states. Actually, the curves shown in Fig. 3 match well the corresponding curves of the SPAC state $|1,\alpha\rangle$ [34]. Thus, we can further verify that in our scheme we can effectively generate the SPAC state if the initial signal input state is in the coherent state with moderate parameter β.

C. Wigner function

To further verify our claim, in this section, we investigate the Wigner function of $|\Theta\rangle$. A state of a quantum-mechanical

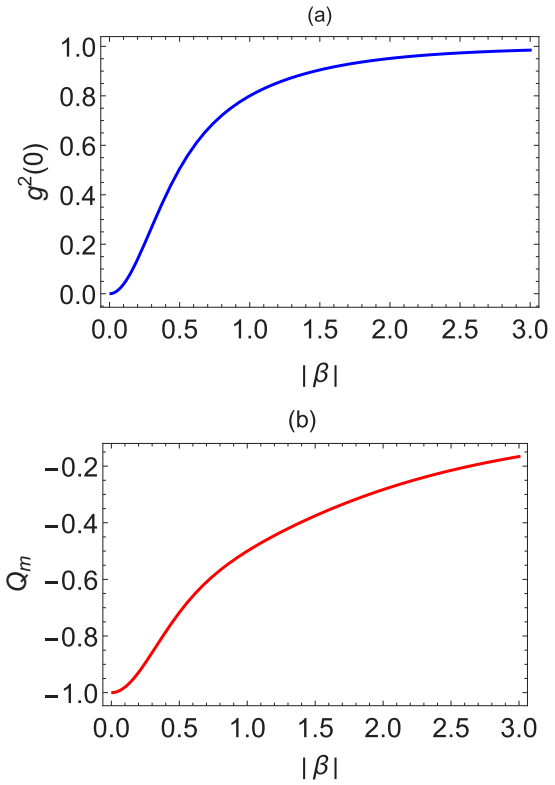

FIG. 3. Second-order correlation $g^{(2)}(0)$ and Mandel factor Q_m of our generated signal output state $|\Theta\rangle$ as a function of the coherent-state parameter $|\beta|$. (a) $g^{(2)}(0)$ is varied. (b) Q_m is varied. Other parameters are the same as in Fig. 2.

system is completely described by the density matrix of a phase-space distribution such as the Wigner function. Every state function has unique phase-space distributions, and the Wigner distribution function is the closest quantum analog of the classical distribution function in phase space. By evaluating the Wigner function we can intuitively determine the strength of the corresponding quantum nature, and most importantly, the negative value of the Wigner function can prove the nonclassicality of the state. In general, the Wigner function is defined as the two-dimensional Fourier transform of the symmetric order characteristic function, and the Wigner function for the state $\rho = |\Theta\rangle\langle\Theta|$ can be written as [67]

$$W(z) \equiv \frac{1}{\pi^2}\int_{-\infty}^{+\infty} \exp(\lambda^* z - \lambda z^*) C_N(\lambda) e^{-\frac{\lambda^2}{2}} d^2\lambda, \qquad (31)$$

where $C_N(\lambda)$ is the normal ordered characteristic function and is defined as

$$C_N(\lambda) = \mathrm{Tr}[\rho e^{\lambda a^\dagger} e^{-\lambda a}]. \qquad (32)$$

After some calculations we can get the explicit expression of the Wigner function of the state $|\Theta\rangle$, which is given as

$$W(z) = \frac{2|\mathcal{N}|^2}{\pi}\Big\{|\kappa_1|^2 e^{-2|z-\beta|^2} - |\kappa_2|^2(1-|2z-\beta|^2)e^{-2|z-\beta|^2} - \mathrm{Re}\Big[\kappa_2\kappa_1^*(2\mathrm{Re}[\beta]-z)e^{\frac{1}{2}[(z-\beta)^2+(z^*-\beta^*)^2]}\Big]\Big\}. \qquad (33)$$

We can see that this Wigner function consists of three parts. The first and second terms corresponded to the Wigner function of the coherent state $|\beta\rangle$ and the SPAC state $|1,\beta\rangle$, respectively, and third term is caused by their superposition. In Fig. 4, we plot the Wigner function of the state $|\Theta\rangle$ for different amplitudes β. From Fig. 4, we can see that the negativity of $W(z)$ vanishes gradually with increasing the amplitude β. We know that every wave function has its phase-space distribution characterized by the Wigner function, and it is unique. The presented phenomenon in Fig. 4 is exactly the phase-space distribution of the SPAC state $|1,\beta\rangle$ [34]. Thus, when $\kappa_2 \gg \kappa_1$, $|\Theta\rangle$ gives us a different type of nonclassical state, i.e., $|1,\beta\rangle$.

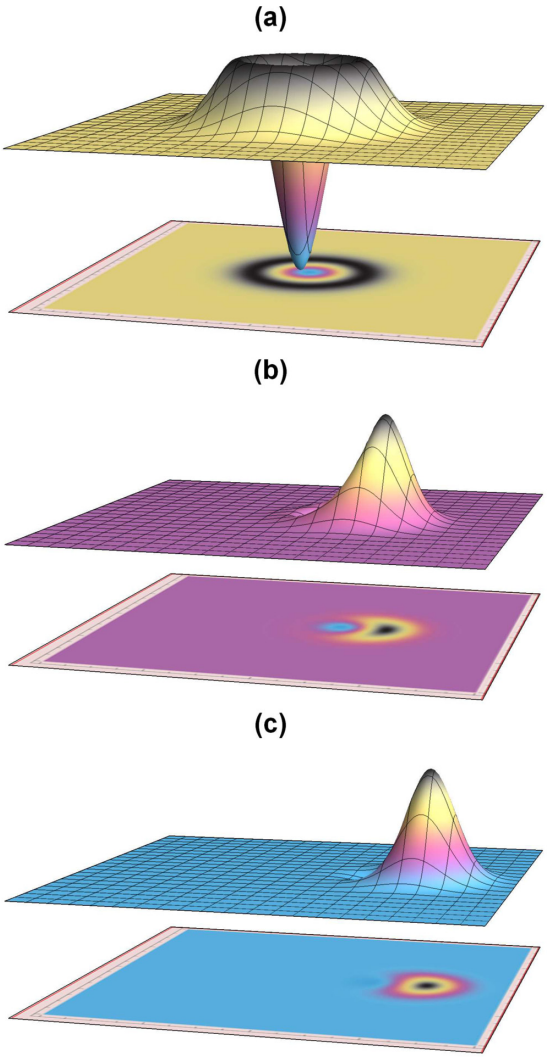

FIG. 4. The Wigner function of the output signal state $|\Theta\rangle$. (a) $|\beta| = 0$, (b) $|\beta| = 1$, and (c) $|\beta| = 2$. Other parameters are the same as in Fig. 2.

D. Signal-to-noise ratio

As shown in our schematic in Fig. 1, the output state $|\Theta\rangle$ of the signal beam is generated after we make the postselection of the idler beam accomplished by D1 and D2. If we did not do the postselection, then the final state of the signal would be given by Eq. (11) after taking a trace of the idler beam with state $|\psi_i\rangle$. However, since in the nonpostselection case

weak values of operators A and B which possess the signal-amplification feature will not occur, the postselected weak measurement may have advantages over the nonpostselected measurement in the signal-amplification process. To show the usefulness of our generated state $|\Theta\rangle$, here we study the ratio of SNRs between the postselected and nonpostselected weak measurements [74],

$$\chi = \frac{\mathcal{R}_X^p}{\mathcal{R}_X^n}. \tag{34}$$

Here $\mathcal{R}_X^p$ represents the SNR of the postselected weak measurement, defined as

$$\mathcal{R}_q^p = \frac{\sqrt{NP_s}\delta q}{\sqrt{\langle q^2\rangle_f - \langle q\rangle_f^2}}, \tag{35}$$

with

$$\delta q = \langle\Theta|q|\Theta\rangle - \langle\beta|q|\beta\rangle. \tag{36}$$

Here N is the total number of measurements; P_s is the probability of finding the postselected state for a given preselected state and, for our scheme, equals $P_s = |\alpha\epsilon|^2$; and NP_s is the number of times the system was found in a postselected state $|\psi_f\rangle$. Here $\langle q\rangle_f$ denotes the expectation value of the measuring observable defined in Eq. (5) under the final state of the pointer (signal beam) $|\Theta\rangle$.

When dealing with nonpostselected measurements, there is no postselection process after the interaction between the system and pointer. Thus, the definition of the SNR for nonpostselected weak measurements can be given as

$$\mathcal{R}_X^n = \frac{\sqrt{N}\delta q'}{\sqrt{\langle q^2\rangle_{f'} - \langle q\rangle_{f'}^2}}, \tag{37}$$

with

$$\delta q' = \langle\Psi|q|\Psi\rangle - \langle\beta|q|\beta\rangle. \tag{38}$$

Here $\langle q\rangle_{f'}$ denotes the expectation value of the measuring observable under the final state of the pointer without postselection, which can be derived in Eq. (11). In order to evaluate the ratio χ of SNRs, we have to calculate the related quantities, and the related expressions are given as follows.

(1) The expectation value of $\langle q\rangle_f$ is

$$\langle q\rangle_f = \langle\Phi|q|\Phi\rangle = \mathcal{N}|^2\{|\kappa_1|^2 h_1 + |\kappa_2|^2 h_2 - 2\mathrm{Re}[\kappa_1\kappa_2^* h_3]\}, \tag{39}$$

where

$$h_1 = \langle\beta|q|\beta\rangle = \sqrt{2}\mathrm{Re}[\beta], \tag{40a}$$

$$h_2 = \langle\beta|aqa^\dagger|\beta\rangle = \sqrt{2}(2+|\beta|^2)\mathrm{Re}[\beta], \tag{40b}$$

$$h_3 = \langle\beta|aq|\beta\rangle = \frac{1}{\sqrt{2}}(1+|\beta|^2+\beta^2). \tag{40c}$$

(2) The expectation value of $\langle q^2\rangle_f$ is

$$\langle q^2\rangle_f = \langle\Phi|q^2|\Phi\rangle = |\mathcal{N}|^2\{|\kappa_1|^2 w_1 + |\kappa_2|^2 w_2 - 2\mathrm{Re}[\kappa_1\kappa_2^* w_2]\}, \tag{41}$$

where

$$w_1 = \langle\beta|q^2|\beta\rangle = \tfrac{1}{2}(2\mathrm{Re}[\beta^2] + 2|\beta|^2 + 1), \tag{42a}$$

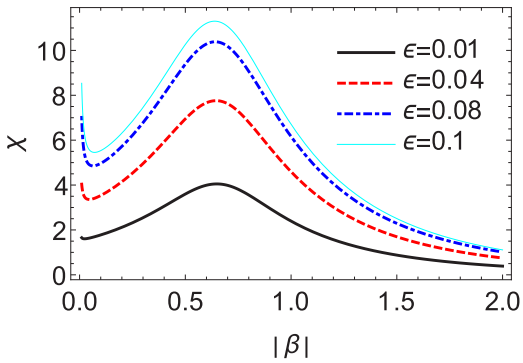

FIG. 5. The ratio χ of SNRs between postselection and nonpostselection weak measurements as a function of the coherent-state parameter β for different values of the slightly unbalanced parameter ϵ of the beam splitter in our scheme. Other parameters are the same as in Fig. 2.

$$w_2 = \langle\beta|aq^2a^\dagger|\beta\rangle = \tfrac{1}{2}(3+7|\beta|^2+2|\beta|^4+2(3+|\beta|^2)\mathrm{Re}[\beta^2]), \tag{42b}$$

$$w_3 = \langle\beta|aq^2|\beta\rangle = \tfrac{1}{2}(3\beta+\beta^3+2\beta^*+\beta^*|\beta|^2+2\beta|\beta|^2). \tag{42c}$$

The other quantities can also be obtained, and here we do not show all of them. The ratio of SNRs between postselected and nonpostselected weak measurements is plotted as a function of the coherent-state parameter β, and the results are shown in Fig. 5. As we observe in Fig. 5, the ratio χ is increased and can be larger than unity with increasing the unbalanced parameter ϵ of the beam splitter for not very large $|\beta|$. We have noticed that the magnitudes of weak values of $\hat{A}$ and $\hat{B}$, Eqs. (15) and (16), are the inverse of ϵ. Thus, the smaller the weak value is, the better the postslected SNR is compared with the nonpostselected one. Briefly, one can draw the conclusion that the postselected weak measurement can improve the SNR better than the case without postselection.

IV. GENERATION OF THE SINGLE-PHOTON-ADDED VACUUM SQUEEZED STATE

We assume the initial input state $|\phi\rangle$ of the signal beam is prepared as the squeeze vacuum state [75]

$$|\phi_1\rangle = S(\xi)|0\rangle, \tag{43}$$

with $S(\xi) = \exp(\frac{1}{2}\xi a^{\dagger 2} - \frac{1}{2}\xi^* a^2)$ and $\xi = \eta e^{i\varphi}$. Then, the output state of the signal beam, Eq. (14), becomes

$$|\Psi\rangle = \chi(|\phi_1\rangle - \lambda_1 a|\phi_1\rangle - \lambda_2 a^\dagger|\phi_1\rangle). \tag{44}$$

Here $\lambda_1 = \frac{g\alpha}{\sqrt{2}}$, $\lambda_2 = \frac{g}{\sqrt{2}\alpha\epsilon}$, and

$$\chi^{-2} = 1 + |\lambda_1|^2\sinh^2\eta - \mathrm{Re}[\lambda_1\lambda_2^* e^{i\theta}]\sinh(2\eta) + |\lambda_2|^2\cosh^2\eta \tag{45}$$

is the normalization constant. In the discussion below, we can neglect the term associated with the coefficient λ_1 since it is too small compared to λ_2 for our allowed parameters. As we can see, the state we prepared by optical modeling $|\Omega\rangle$ is the superposition of the vacuum squeezed (VS) and

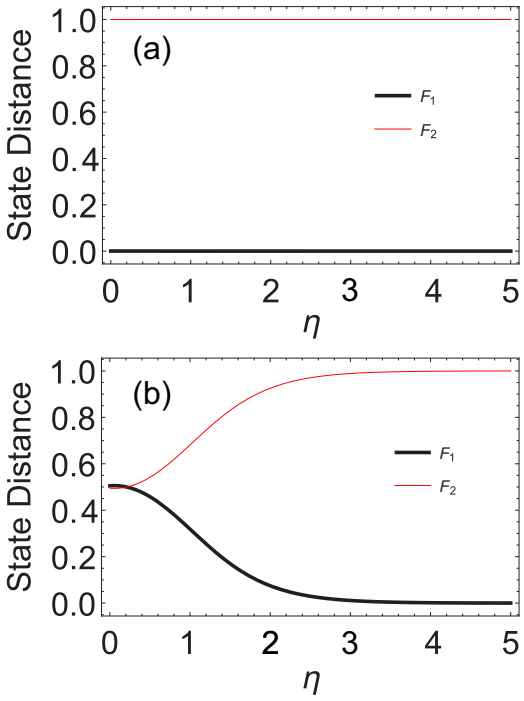

FIG. 6. The state distance of $|\Omega\rangle$ between SVS and PASVS as a function of the squeezed-state parameter η (a) for $\alpha = 0.01$ and (b) for $\alpha = 0.75$. Other parameters are the same as in Fig. 2.

single-photon-added vacuum squeezed (SPAVS) states. These two states' dominance depends on the coefficients λ_1, and their amplitudes can be controlled by beam splitters and the BBO crystal in our scheme (see Fig. 1). The states generated by excitations on a squeezed vacuum state have some interesting nonclassical properties [76,77] and have potential applications that include entanglement distillation [78–80], the fidelity of continuous-variable teleportation [81,82], and nonlocality [83]. In this section, by calculating the state distance, squeezing parameter, and Wigner function we prove that in the allowed parameter region our generated state $|\Omega\rangle$ is very distinguishable over the initial input state $|\phi_1\rangle$.

A. State distance

In order to investigate the similarities and differences of the generated state $|\Omega\rangle$ between the SV state and SPASV state, we evaluate the state distances between them.

(1) The state distance between $|\Omega\rangle$ and the SV state$|\phi_1\rangle$ is given as

$$F_1 = |\langle\xi|\Psi\rangle|^2 = |\chi|^2. \tag{46}$$

(2) The state distance between $|\Omega\rangle$ and the SPASV state $|\phi_2\rangle = \frac{a^\dagger|\xi\rangle}{\cosh\eta}$ is given as

$$F_2 = |\langle\phi_2|\Psi\rangle|^2 = \left|\frac{\chi}{\cosh\eta}\right|^2 \left|\frac{1}{2}e^{i\theta}\lambda_1 \sinh 2\eta - \lambda_2 \cosh^2\eta\right|^2. \tag{47}$$

In Fig. 6, we plot separately the state distances between $|\Omega\rangle$ and the two states vs the squeezing parameter η. As indicated in Fig. 6(a), when the input idler coherent state is too weak, $\alpha = 0.01$, the output signal state $|\Omega\rangle$ is very different from the initial input state, and the generated state is totally the same as the SPASV state. For $\alpha = 0.75$, for a very weak squeezing parameter η, the output state $|\Omega\rangle$ is very similar to the SV and SPASV states. But with increasing the squeezing parameter η, the similarities between $|\Omega\rangle$ and the SPASV (SV) state are increased(decreased) significantly [see Fig. 6(b)]. Although the SPASV state is only one photon different from the SV state, it has very different features from the SV state. Next, we study the squeezing parameter and Wigner functions of our generated state $|\Omega\rangle$. We notice that in Ref. [84] the authors proposed a scheme to generate a photon-added SV state by mixing the SV state with a single-photon state on a low-reflectivity beam splitter. But that process is highly nondeterministic and less efficient than the scheme we present here.

B. Squeezing parameter

As we know, the SV state is an ideal state which possesses a very strong squeezing effect. To investigate the squeezing effect of the field quadrature of the generated state $|\Omega\rangle$, in this section we study the squeezing parameter of $|\Omega\rangle$. The squeezing parameter of the radiation field is defined as

$$S_\phi = (\triangle X_\phi)^2 - \tfrac{1}{2}, \tag{48}$$

where

$$\hat{X}_\phi = \frac{1}{\sqrt{2}}(ae^{-i\phi} + a^\dagger e^{i\phi}), \quad \phi \in [0, 2\pi], \tag{49}$$

is the quadrature operator of the field and $\triangle X_\phi = \sqrt{\langle\hat{X}_\phi^2\rangle - \langle\hat{X}_\phi\rangle^2}$ is the variance of variable X_θ. The minimum value of S_ϕ is -0.5, and if $-0.5 \leqslant S_\phi < 0$, the field is called nonclassical. We can calculate the squeezing parameters of the SV state $|\phi_1\rangle$, SPASV state $|\phi_2\rangle$, and generated output state $|\Omega\rangle$ easily, and their curves are given in Fig. 7. We observe from Fig. 7(a) that when $\alpha = 0.01$, the squeezing parameter of the generated output signal state $|\Omega\rangle$ is exactly the same as the squeezing parameter of the SPASV state $|\phi_2\rangle$, and it has very good squeezing in the initial input state $|\phi_1\rangle$ when the squeezing parameter η becomes larger. Furthermore, as shown in Fig. 7(b), if $\alpha = 0.75$, then the squeezing parameter of $|\Omega\rangle$ is the same as the initial input state $|\phi_1\rangle$. Here we have to mention that in our scheme it is required that the measured system is initially prepared in a very weak coherent state. Thus, the $\alpha = 0.75$ case is not our main point.

C. Wigner function of the generated state

To further confirm the similarities between the SPASV state $|\phi_2\rangle$ and the generated state $|\Omega\rangle$, in this section we study the Wigner function of $|\Omega\rangle$. The Wigner function for the state $\rho = |\Omega\rangle\langle\Omega|$ can be written as [67]

$$W(z) \equiv \frac{1}{\pi^2}\int_{-\infty}^{+\infty} \exp(\lambda^* z - \lambda z^*) C_W(\lambda) d^2\lambda. \tag{50}$$

Here $C_W(\lambda)$ is the characteristic function and is defined as

$$C_W(\lambda) = \mathrm{Tr}[\rho e^{\lambda a^\dagger - \lambda^* a}], \tag{51}$$

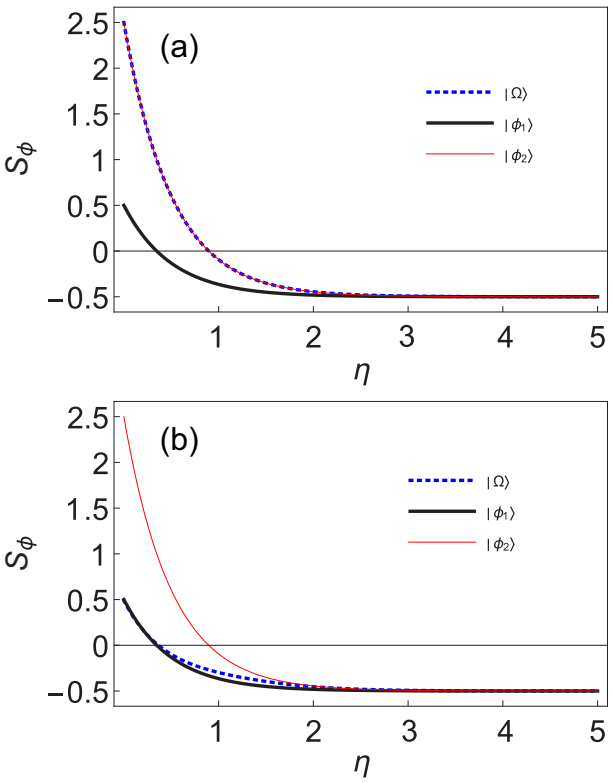

FIG. 7. The squeezing parameter S_ϕ of $|\Omega\rangle$, the SV state $|\phi_1\rangle$, and the SPASV state $|\phi_2\rangle$ vs the squeezing parameter η (a) for $\alpha = 0.01$ and (b) for $\alpha = 0.75$. Here we take $\phi = 0$, and other parameters are the same as in Fig. 2.

and $z = x + ip$ represents the normalized dimensionless position and momentum observables of the beam in phase space. After some math, we can calculate the explicit expression of the Wigner function of the generated state $|\Omega\rangle$, which reads

$$W(z) = |\chi|^2 w_1(z) + |\lambda_1|^2|\chi|^2 w_2(z) + |\lambda_2|^2|\chi|^2 w_3(z) - 2|\chi|^2 \mathrm{Im}[\lambda_1 e^{i\varphi}] w_4(z) - 2\mathrm{Im}[\lambda_2]|\chi|^2 w_5(z) - 2|\chi|^2 \mathrm{Re}[\lambda_1^* \lambda_2 e^{-i\varphi}] w_6(z), \quad (52)$$

with

$$w_1(z) = \frac{2}{\pi} \exp[-2|\tilde{z}|^2], \quad (53a)$$

$$w_2(z) = \frac{2}{\pi} \sinh^2 \eta \exp^{-2|\tilde{z}|^2}(4|\tilde{z}|^2 - 1), \quad (53b)$$

$$w_3(z) = \frac{2}{\pi} \cosh^2 \eta \exp^{-2|\tilde{z}|^2}(4|\tilde{z}|^2 - 1), \quad (53c)$$

$$w_4(z) = \frac{4}{\pi} \mu \sinh \eta e^{-\tau}, \quad (53d)$$

$$w_5(z) = \frac{4}{\pi} \mu^* \cosh \eta e^{-\tau}, \quad (53e)$$

$$w_6(z) = \frac{1}{\pi} \sinh 2\eta \exp^{-2|\tilde{z}|^2}(4|\tilde{z}|^2 - 1). \quad (53f)$$

Here $\tilde{z} = z\cosh\eta - z^* e^{i\theta}\sinh\eta$, $\tau = 2(\mathrm{Re}[z])^2(\cosh\eta - \sinh\eta)^2 - 2(\mathrm{Im}[z])^2(\cosh\eta + \sinh\eta)^2$, and $\mu = \mathrm{Re}[z](\sinh\eta - \cosh\eta) + i\mathrm{Im}[z](\sinh\eta + \cosh\eta)$. We can observe that this Wigner function is a real function, and its value is bounded by $-\frac{2}{\pi} \leqslant W(\alpha) \leqslant \frac{2}{\pi}$ in the whole phase space. In the derivation of the above Wigner function we have used the identities

$$S(\xi) a S^\dagger(\xi) = a\cosh(\eta) - a^\dagger e^{i\varphi}\sinh(\eta), \quad (54a)$$

$$S(\xi) a^\dagger S^\dagger(\xi) = a^\dagger\cosh(\eta) - a e^{-i\varphi}\sinh(\eta). \quad (54b)$$

$w_2(z)$ in the Wigner function (52) is the Wigner function of the SV state $|\phi_1\rangle$. Although the SV state $|\phi_1\rangle$ is a nonclassical state, its Wigner function is Gaussian and positive in phase space [35]. It is very clear in Eq. (52) that it contains non-Gaussian terms such as $w_2(z)$, $w_3(z)$, and $w_6(z)$. Thus, the Wigner function of our generated signal state is non-Gaussian in the phase space. We present the plots of the Wigner functions of the initial input signal state $|\phi_1\rangle$, our generated output signal state $|\Omega\rangle$, and the SPASV state $|\phi_2\rangle$ in phase space in Fig. 8 for different squeezing parameters which we set as $\eta = 0, 1, 2$. Figures 8(a)–8(c) represent Wigner functions of the SV state $|\phi_1\rangle$, Figs. 8(d)–8(f) represent Wigner functions of the generated state $|\Omega\rangle$, and Figs. 8(g)–8(i) represent Wigner functions of the SPASV state $|\phi_2\rangle$. By comparing the curves of those Wigner functions, we observe that the generated state in our scheme is a nonclassical state. It is very clear from Figs. 8(d)–8(f) that as the initial input state $|\phi_1\rangle$, the state $|\Omega\rangle$ has squeezing in one of the quadratures, and there are also some negative regions of the Wigner functions in the phase space. These two features of the state $|\Omega\rangle$ show its nonclassicality. Furthermore, it is proved that our generated state $|\Omega\rangle$ has exactly the same phase-space distribution as the SPASV state $|\phi_2\rangle$ (see the second and third rows of Fig. 8). As indicated in Fig. 8(d), if the input state of the pointer is a vacuum, then the output signal state is prepared in the single-photon Fock state.

V. CONCLUSION

In summary, we have designed a fully laboratory feasible optical model to successfully prepare nonclassical states such as the single-photon Fock state, SPAC state, and SPASV state by using postselected weak measurements in a three-wave mixing process. In our scheme the signal and idler beams are taken as the pointer and measured system, respectively, and entanglement between them is realized by a BBO crystal which can play the role of weak measurement. In other words, in our study, a nonlinear BBO crystal was chosen to introduce weak interaction in three-wave mixing including pump, idle, and signal light. By making the pre- and postselections in the measured system, the final pointer state is the desired nonclassical state which depends on the initial input signal state (initial pointer state). Further, we investigated other properties, including squeezing, second-order correlation, and Wigner functions of conditional output states.

We found that if the input signal (pointer) is the vacuum state, then the output signal state is prepared in the single-photon Fock state, which is a typical quantum state

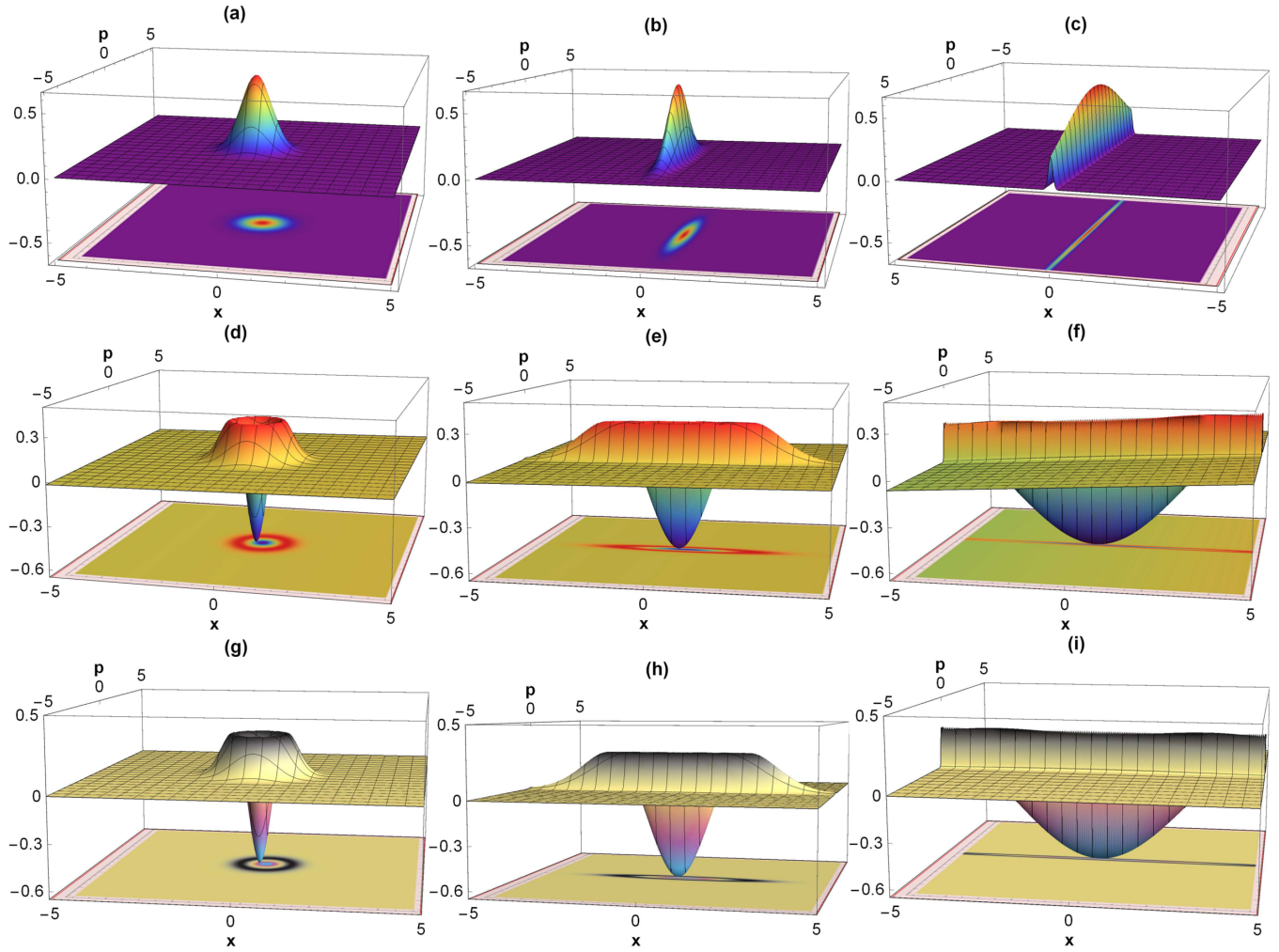

FIG. 8. Comparison of the Wigner functions of the SV state $|\phi_1\rangle$, the SPASV state $|\phi_2\rangle$, and the generated state $|\Omega\rangle$ in phase space. Each column is defined by a different value of the squeezing parameter η (set $\eta = 0, 1, 2$), and they are ordered accordingly from left to right. (a)–(c) correspond to the Wigner functions of the initial input SV state $|\phi_1\rangle$, (d)–(f) correspond to the Wigner functions of the generated output signal state $|\Omega\rangle$, and (g)–(i) correspond to the Wigner functions of the SPASV state $|\phi_2\rangle$. Other parameters are the same as in Fig. 2.

exclusively used in many quantum information processes. We also found that if the input signal state is a coherent (squeezed vacuum) state, then the output signal state is prepared in the SPAC (SPAVS) state, and their purities can easily be controlled by optical elements. Furthermore, we also found that the postselective measurement characterized by weak values and postselection has a positive effect on the output SNR over nonpostselection for the coherent-state input case.

Our scheme for the preparation of nonclassical states can be implemented in optical laboratories, and we anticipate that this scheme could provide other effective methods for the generation of other useful nonclassical state such as Schrödinger's kitten states [13].

ACKNOWLEDGMENTS

This work was supported by the National Natural Science Foundation of China (Grant No. 11865017), the Natural Science Foundation of Xinjiang Uyghur Autonomous Region (Grant No. 2020D01A72), and the Introduction Program of High Level Talents of Xinjiang Ministry of Science.

[1] S. Haroche and J.-M.Raimond, *Exploring the Quantum: Atoms, Cavities, and Photons* (Oxford University Press, Oxford, 2006).

[2] S. P. Walborn, M. P. Almeida, P. H. S. Ribeiro, and C. H. Monken, Quantum Inf. Comput. **6**, 336 (2006).

[3] M. A. Nielsen and I. L.Chuang, *Quantum Computation and Quantum Information* (Cambridge University Press, Cambridge, 2010).

[4] H. Yonezawa and A. Furusawa, Opt. Spectrosc. **108**, 288 (2010).

[5] Z. Zhang and L. M. Duan, New J. Phys. **16**, 103037 (2014).

[6] A. Blais, S. M. Girvin, and W. D. Oliver, Nat. Phys. **16**, 247 (2020).

[7] J. I. Cirac, R. Blatt, A. S. Parkins, and P. Zoller, Phys. Rev. Lett. **70**, 762 (1993).

[8] P. Bertet, S. Osnaghi, P. Milman, A. Auffeves, P. Maioli, M. Brune, J. M. Raimond, and S. Haroche, Phys. Rev. Lett. **88**, 143601 (2002).

[9] M. Hofheinz, E. M. Weig, M. Ansmann, R. C. Bialczak, E. Lucero, M. Neeley, A. D. O'Connell, H. Wang, J. M. Martinis, and A. N. Cleland, Nature (London) **454**, 310 (2008).

[10] B. Wang and L.-M. Duan, Phys. Rev. A **72**, 022320 (2005).

[11] A. Ourjoumtsev, R. Tualle-Brouri, J. Laurat, and P. Grangier, Science **312**, 83 (2006).

[12] A. Ourjoumtsev, H. Jeong, R. Tualle-Brouri, and P. Grangier, Nature (London) **448**, 784 (2007).

[13] B. Vlastakis, G. Kirchmair, Z. Leghtas, S. E. Nigg, L. Frunzio, S. M. Girvin, M. Mirrahimi, M. H. Devoret, and R. J. Schoelkopf, Science **342**, 607 (2013).

[14] T. Serikawa, J.-I. Yoshikawa, S. Takeda, H. Yonezawa, T. C. Ralph, E. H. Huntington, and A. Furusawa, Phys. Rev. Lett. **121**, 143602 (2018).

[15] B. Hacker, S. Welte, S. Daiss, A. Shaukat, S. Ritter, L. Li, and G. Rempe, Nat. Photonics **13**, 110 (2019).

[16] L. Duan, Nat. Photonics **13**, 73 (2019).

[17] W. S. Leong, M. Xin, Z. Chen, S. Chai, Y. Wang, and S.-Y. Lan, Nat. Commun. **11**, 5295 (2020).

[18] M. Lewenstein, M. F. Ciappina, E. Pisanty, J. Rivera-Dean, P. Stammer, T. Lamprou, and P. Tzallas, Nat. Phys. **17**, 1104 (2021).

[19] G. Breitenbach, S. Schiller, and J. Mlynek, Nature (London) **387**, 471 (1997).

[20] C. K. Hong and L. Mandel, Phys. Rev. Lett. **56**, 58 (1986).

[21] J. Krause, M. O. Scully, and H. Walther, Phys. Rev. A **36**, 4547 (1987).

[22] F. W. Cummings and A. K. Rajagopal, Phys. Rev. A **39**, 3414 (1989).

[23] B. T. H. Varcoe, S. Brattke, M. Weidinger, and H. Walther, Nature (London) **403**, 743 (2000).

[24] Y. Liu, L. F. Wei, and F. Nori, Europhys. Lett. **67**, 941 (2004).

[25] E. Waks, E. Diamanti, and Y. Yamamoto, New J. Phys. **8**, 4 (2006).

[26] A. A. Houck, D. I. Schuster, J. M. Gambetta, J. A. Schreier, B. R. Johnson, J. M. Chow, L. Frunzio, J. Majer, M. H. Devoret, S. M. Girvin, and R. J. Schoelkopf, Nature (London) **449**, 328 (2007).

[27] M. Moussa and B. Baseia, Phys. Lett. A **238**, 223 (1998).

[28] R. Lo Franco, G. Compagno, A. Messina, and A. Napoli, Open Syst. Inf. Dyn. **13**, 463 (2006).

[29] R. Lo Franco, G. Compagno, A. Messina, and A. Napoli, Phys. Lett. A **374**, 2235 (2010).

[30] J. S. Neergaard-Nielsen, B. M. Nielsen, C. Hettich, K. Mølmer, and E. S. Polzik, Phys. Rev. Lett. **97**, 083604 (2006).

[31] H. Takahashi, K. Wakui, S. Suzuki, M. Takeoka, K. Hayasaka, A. Furusawa, and M. Sasaki, Phys. Rev. Lett. **101**, 233605 (2008).

[32] S.-Y. Liu, Y.-Z. Li, L.-Y. Hu, J.-H. Huang, X.-X. Xu, and X.-Y. Tao, Laser Phys. Lett. **12**, 045201 (2015).

[33] X.-X. Xu and H.-X. Yuan, Quantum Inf. Process. **19**, 324 (2020).

[34] G. S. Agarwal and K. Tara, Phys. Rev. A **43**, 492 (1991).

[35] A. Biswas and G. S. Agarwal, Phys. Rev. A **75**, 032104 (2007).

[36] R. Carranza and C. C. Gerry, J. Opt. Soc. Am. B **29**, 2581 (2012).

[37] Y. Wang, W.-S. Bao, H.-Z. Bao, C. Zhou, M.-S. Jiang, and H.-W. Li, Phys. Lett. A **381**, 1393 (2017).

[38] M. Miranda and D. Mundarain, Quantum Inf. Process. **16**, 298 (2017).

[39] J.-J. Chen, C.-H. Zhang, J.-M. Chen, C.-M. Zhang, and Q. Wang, Quantum Inf. Process. **19**, 198 (2020).

[40] J. Fiurášek, R. García-Patrón, and N. J. Cerf, Phys. Rev. A **72**, 033822 (2005).

[41] A. Zavatta, S. Viciani, and M. Bellini, Science **306**, 660 (2004).

[42] A. Zavatta, S. Viciani, and M. Bellini, Phys. Rev. A **72**, 023820 (2005).

[43] H. Jeong, A. M. Lance, N. B. Grosse, T. Symul, P. K. Lam, and T. C. Ralph, Phys. Rev. A **74**, 033813 (2006).

[44] M. Barbieri, N. Spagnolo, M. G. Genoni, F. Ferreyrol, R. Blandino, M. G. A. Paris, P. Grangier, and R. Tualle-Brouri, Phys. Rev. A **82**, 063833 (2010).

[45] X. Xu and H. Yuan, arXiv:1911.10945.

[46] D. Stoler and B. Yurke, Phys. Rev. A **34**, 3143 (1986).

[47] K. Watanabe and Y. Yamamoto, Phys. Rev. A **38**, 3556 (1988).

[48] M. Brune, S. Haroche, V. Lefevre, J. M. Raimond, and N. Zagury, Phys. Rev. Lett. **65**, 976 (1990).

[49] M. Ueda and M. Kitagawa, Phys. Rev. Lett. **68**, 3424 (1992).

[50] M. Ban, Phys. Rev. A **49**, 5078 (1994).

[51] M. Dakna, T. Anhut, T. Opatrný, L. Knöll, and D.-G. Welsch, Phys. Rev. A **55**, 3184 (1997).

[52] M. Takeoka and M. Sasaki, Phys. Rev. A **75**, 064302 (2007).

[53] S. M. Barnett, G. Ferenczi, C. R. Gilson, and F. C. Speirits, Phys. Rev. A **98**, 013809 (2018).

[54] Y. Aharonov, D. Z. Albert, and L. Vaidman, Phys. Rev. Lett. **60**, 1351 (1988).

[55] J. Dressel, M. Malik, F. M. Miatto, A. N. Jordan, and R. W. Boyd, Rev. Mod. Phys. **86**, 307 (2014).

[56] A. G. Kofman, S. Ashhab, and F. Nori, Phys. Rep. **520**, 43 (2012).

[57] K. Nakamura, A. Nishizawa, and M.-K. Fujimoto, Phys. Rev. A **85**, 012113 (2012).

[58] Y. Turek, H. Kobayashi, T. Akutsu, C.-P. Sun, and Y. Shikano, New J. Phys. **17**, 083029 (2015).

[59] Y. Turek, W. Maimaiti, Y. Shikano, C.-P. Sun, and M. Al-Amri, Phys. Rev. A **92**, 022109 (2015).

[60] Y. Turek, Chin. Phys. B **29**, 090302 (2020).

[61] Y. Turek, Eur. Phys. J. Plus **136**, 221 (2021).

[62] A. Feizpour, X. Xing, and A. M. Steinberg, Phys. Rev. Lett. **107**, 133603 (2011).

[63] A. Feizpour, M. Hallaji, G. Dmochowski, and A. M. Steinberg, Nat. Phys. **11**, 905 (2015).

[64] F. Matsuoka, A. Tomita, and Y. Shikano, Quantum Stud.: Math Found. **4**, 159 (2017).

[65] S. Roy, J. T. Chalker, I. V. Gornyi, and Y. Gefen, Phys. Rev. Research **2**, 033347 (2020).

[66] P. Kumar, K. Snizhko, and Y. Gefen, Phys. Rev. Res. **2**, 042014(R) (2020).

[67] C. Gerry and P. Knight, *Introductory Quantum Optics* (Cambridge University Press, Cambridge, 2004).

[68] B. Yurke, S. L. McCall, and J. R. Klauder, Phys. Rev. A **33**, 4033 (1986).

[69] S. Wu and M. Żukowski, Phys. Rev. Lett. **108**, 080403 (2012).

[70] P. V. P. Pinheiro and R. V. Ramos, Quantum Inf. Process. **12**, 537 (2013).

[71] S. Srikara, K. Thapliyal, and A. Pathak, Quantum Inf. Process. **19**, 371 (2020).
[72] J.-R. Zhu, C.-Y. Wang, K. Liu, C.-M. Zhang, and Q. Wang, Quantum Inf. Process. **17**, 294 (2018).
[73] A. Uhlmann, Rep. Math. Phys. **9**, 273 (1976).
[74] G. Agarwal, *Quantum Optics* (Cambridge University Press, Cambridge, 2013).
[75] D. F. Walls, Nature (London) **306**, 141 (1983).
[76] Z. Zhang and H. Fan, Phys. Lett. A **165**, 14 (1992).
[77] X. Xu, H. Yuan, and L. Zhou, Opt. Commun. **335**, 133 (2015).
[78] J. Fiurášek, Phys. Rev. A **82**, 042331 (2010).
[79] J. Fiurášek, Phys. Rev. A **84**, 012335 (2011).
[80] S. L. Zhang and P. van Loock, Phys. Rev. A **82**, 062316 (2010).
[81] T. Opatrný, G. Kurizki, and D.-G. Welsch, Phys. Rev. A **61**, 032302 (2000).
[82] Y. Yang and F.-L. Li, Phys. Rev. A **80**, 022315 (2009).
[83] H. Nha and H. J. Carmichael, Phys. Rev. Lett. **93**, 020401 (2004).
[84] J. P. Olson, K. P. Seshadreesan, K. R. Motes, P. P. Rohde, and J. P. Dowling, Phys. Rev. A **91**, 022317 (2015).